Systematic investigation of channel-coupling effects on elastic, inelastic, and neutron-transfer channels in ^{6}Li + ^{159}Tb

Saikat Bhattacharjee,[1,2] Piyasi Biswas,[1,2,*] Ashish Gupta,[1,2] M. K. Pradhan,[1,†] N. Deshmukh,[1,‡] P. Basu,[1,§] V. V. Parkar,[3,2] S. Santra,[3,2] K. Ramachandran,[3] A. Chatterjee,[3] Subinit Roy,[1,§] and A. Mukherjee[1,2,‖]

[1]*Saha Institute of Nuclear Physics, 1/AF, Bidhan Nagar, Kolkata-700064, India*

[2]*Homi Bhabha National Institute, Mumbai-400094, India*

[3]*Nuclear Physics Division, Bhabha Atomic Research Centre, Mumbai-400085, India*

(Received 14 October 2022; accepted 7 November 2022; published 23 December 2022)

Elastic-scattering angular distribution for the weakly bound nucleus ^{6}Li on the deformed rare-earth ^{159}Tb target nucleus has been measured at energies around the Coulomb barrier. The elastic-scattering cross sections for this reaction consist of inelastic contributions from low-lying excited states of ^{159}Tb. The pure elastic cross sections have been extracted from the admixture of elastic and inelastic data. The optical model potential parameters for the system have been obtained from the extracted pure elastic-scattering cross sections. Coupled-channel calculations have been performed with this set of potential parameters, to compare the theoretical and experimental inelastic-scattering cross sections. The work has been extended to obtain the spectroscopic factor for ^{158}Tb + n configuration from the experimental 1n-pickup data.

DOI: 10.1103/PhysRevC.106.064612

I. INTRODUCTION

The reaction process between two heavy ions has been studied extensively over the last few decades at energies around the Coulomb barrier to get a deeper understanding of the nuclear potential. In recent years, the study of the nuclear potential has been focused on stable weakly bound nuclei at energies around the Coulomb barrier [1–29]. Because of their prevalent cluster structure, nuclear reactions involving the weakly bound nuclei have an increased probability of breakup and transfer [30]. The systematics of such increased transfer and breakup probability influences the elastic-scattering cross sections [31]. Consequently, the mean-field potential extracted from the elastic-scattering measurement is also affected due to the increased probability of breakup and transfer, which is reflected in the energy dependence of the optical model potential. The near threshold behavior of the potential, known as the threshold anomaly (TA) [32], exhibits a different behavior for the weakly bound projectiles, unlike the strongly bound systems [7,8].

Highly deformed rare-earth nuclei [33] like ^{159}Tb have large density of excited states adjacent to the ground state. Elastic-scattering measurements involving these nuclei generally yield quasielastic data, an admixture of elastic and inelastic scattering to low-lying states. Subsequently, a statistical model can be implemented to extract the elastic-scattering cross sections from the quasielastic data [34].

Measurements of fusion [35], α yield [36], and quasielastic barrier distribution [37] have been reported for ^{6}Li + ^{159}Tb systems. However, the elastic-scattering measurement for ^{6}Li + ^{159}Tb does not exist in the literature, and the study of ^{7}Li + ^{159}Tb [26] exhibits unusual energy dependence of optical model potential parameters. In that scenario, elastic-scattering measurement for the weakly bound ^{6}Li projectile on the permanently deformed rare-earth nucleus ^{159}Tb as the target has been presented in this work. The work further extends to probe the one-neutron (1n) pickup channel in the reaction of ^{6}Li + ^{159}Tb.

Section II of this paper consists of the experimental details, analytical procedures to extract the elastic part from quasielastic data, and the search for optical model potential parameters. Section III recounts the theoretical calculations that have been performed to reproduce the quasielastic and transfer data at different energies. A summary of the present work and concluding remarks are included in Sec. IV.

II. EXPERIMENTAL DETAILS AND ANALYSIS

A. Experimental details

The experiment has been performed at the 14UD BARC-TIFR Pelletron Accelerator at TIFR, Mumbai. Beams of ^{6}Li with laboratory energies 25, 27, 30, and 35 MeV have been used to bombard a self-supporting rolled target foil of ^{159}Tb with thickness of 700 μg/cm^{2}. Four silicon (Si) surface bar-

*Present address: Shahid Matangini Hazra Government College for Women, Tamluk, Chakshrikrishnapur, Kulberia, Purba Medinipur, West Bengal - 721649, India.

†Present address: Department of Physics, Belda College, Belda, Paschim Medinipur, West Bengal - 721424.

‡Present address: School of Sciences, Auro University, Surat, Gujarat - 394510, India.

§Retired.

‖anjali.mukherjee@saha.ac.in.

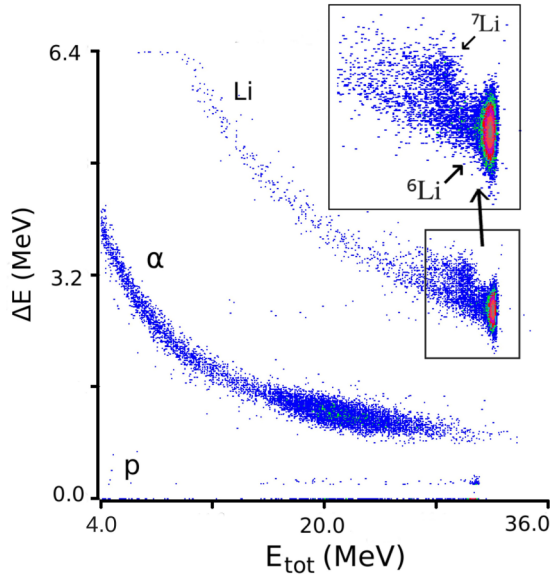

FIG. 1. Typical ΔE-$E_{\rm tot}$ spectra for scattering of ^{6}Li + ^{159}Tb system at $E_{\rm lab} = 35$ MeV and $\theta_{\rm lab} = 59.5^{\circ}$. The uppermost band, with an enlarged view in the inset; consists of scattered ^{6}Li projectile, either elastically or inelastically; and ^{7}Li emerging from $1n$ pickup of ^{6}Li.

rier ΔE-E telescope detectors were employed in an angular range $20^{\circ} \leqslant \theta_{\rm lab} \leqslant 160^{\circ}$ to detect the scattered particles at different angles. The thicknesses of the four ΔE-E detectors are 25–500 μm, 25–2000 μm, 25–3000 μm, and 25–2000 μm, respectively. Two monitor detectors were placed at $\pm 10^{\circ}$ with respect to the beam direction for normalizing purposes. A typical $\Delta E - E_{\rm tot}$ spectrum ($E_{\rm tot}$ corresponds to the sum of energies deposited in ΔE and E detectors) is shown in Fig. 1. The ^{6}Li band in Fig. 1 is the elastic-scattering band. At the top of the ^{6}Li, the formation of a ^{7}Li blob represents the $1n$ pickup channel. The Linux-based data-acquisition system LAMPS [38] has been employed to register the data.

B. Extraction of elastic-scattering data

The ^{159}Tb nucleus is highly deformed with an unpaired proton coupling with the 0^{+}, 2^{+}, ... pure rotational states. As a consequence, the nucleus ^{159}Tb has low-lying excited states at 58 keV, 137 keV, and so on. The Si surface barrier detectors used in the experiment have an estimated energy resolution of ≈150 keV. Hence, contribution of inelastic scattering by the low-lying excited states of the target cannot be separated by experimental means. Thus, the largest blob in the Li band (see Fig. 1) will consist of contributions from inelastic scattering. It is therefore requisite to separate the pure elastic-scattering data from the admixture of elastic and inelastic-scattering data. In Fig. 2, the measured quasielastic angular distribution cross sections at energies $E_{\rm lab} = 25$, 27, 30z, and 35 MeV have been presented. The factor $\sigma_{\rm qel}/\sigma_{\rm Ruth}$ in Fig. 2 represents the quasielastic differential scattering cross sections normalized to the Rutherford cross section.

A one-dimensional projection of the Li band is shown in Fig. 3. The peak is fit by the statistical double Gaussian fitting

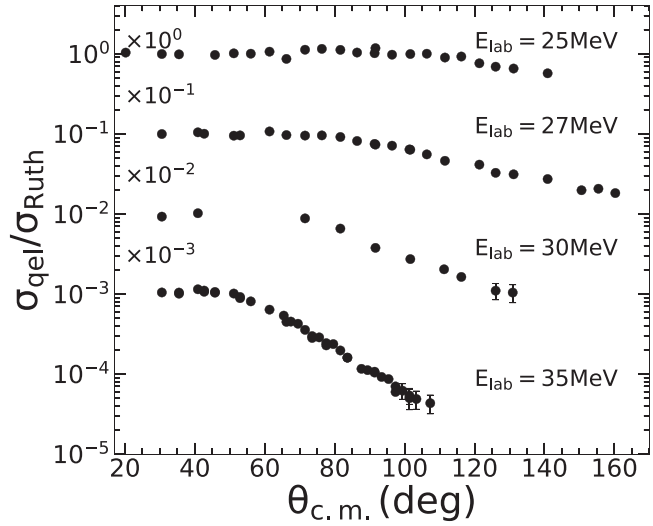

FIG. 2. Experimental angular distribution of quasielastic scattering cross sections at different incident energies for ^{6}Li + ^{159}Tb system.

method to disentangle the elastic data (see Fig. 3). The fitting was done with the following constraints:

(1) The peak of the second Gaussian will be at an energy which is 58 keV less than the peak of elastic scattering. The first-excited state of ^{159}Tb is 58 keV above the ground state. Imposing this condition takes care of the peak position of the first inelastic state.
(2) The full width at half maximum (FWHM) of the two peaks of the double Gaussian will be same. This condition comes from the fact that the energy resolution

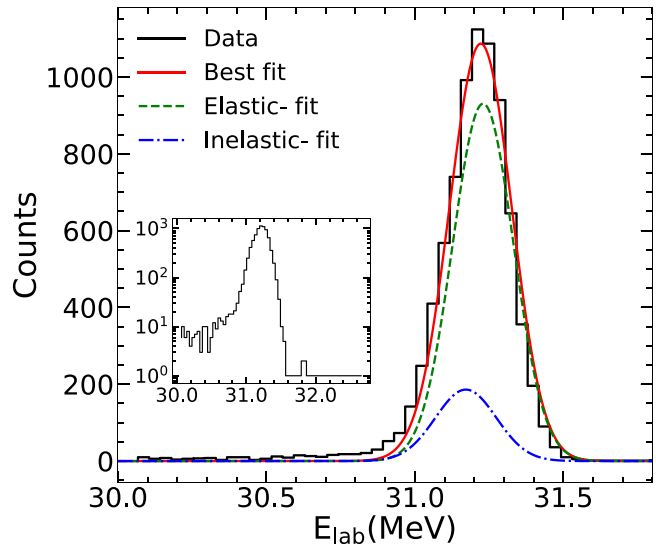

FIG. 3. Result of double Gaussian fit performed on the elastic + inelastic data (at $\theta_{\rm lab} = 75.5^{\circ}$, $E_{\rm lab} = 35$ MeV). The elastic data extracted (dashed lines) from the fit has been used to obtain the model potential parameters of the system. (inset) Deviation of the data from the Gaussian shape can be observed, which indicates an admixture of elastic and inelastic cross section.

of the detector, which is roughly equal to the FWHM of the peaks does not change significantly over a difference of 58 keV in energy.

(3) Ratios of elastic-to-inelastic cross section at different angles have been estimated from the initial coupled-channel calculations employing different global potentials [39,40]. The experimental single-particle transition strengths for ^{159}Tb have been incorporated in the calculations to fix the ratio. During the fitting procedure, the ratios have been maintained to obtain a more reliable result.

It should be noted that the contribution from the second inelastic state of ^{159}Tb; situated at 137 keV above the ground state, is also present within the data. But including a third Gaussian in the fitting algorithm was not feasible as the Gaussian peaks could not be distinguished. Furthermore, including another Gaussian would increase the number of free parameters, rendering the fitting less accurate; as different combinations of the parameters may yield the same result. Thus, the extracted elastic and inelastic parts probably still consists of contribution from the 137 keV inelastic state. The fitting has been performed with the aid of χ^2-minimization method. The technique has been successfully carried out at above barrier energies at scattering angles where the ratio of inelastic- to elastic-scattering cross section is greater than 3%−4%. At energies below the Coulomb barrier, the ratio of inelastic- to elastic-scattering cross section becomes smaller (<3%−4%) even at higher angles, which cannot be resolved statistically. The attribute becomes more prominent with decreasing energies. In these circumstances, the total cross sections estimated from the raw data have been considered to come from elastic scattering only. Errors in the fit parameters as well as the statistical error of the data have been taken into account while calculating the overall error for the elastic and inelastic components. As the errors of the data points include error originating from the double Gaussian fit along with the statistical error of counts, the error bars associated with the data points are higher than that usual.

The ratio of elastic to Rutherford differential cross section is then expressed as

$$\frac{d\sigma_{\rm el}}{d\sigma_{\rm Ruth}}(E,\theta_{\rm tel}) = \frac{Y_{\rm el}(E,\theta_{\rm tel})}{Y_m(E,\theta_m)} \times \frac{(d\sigma_{\rm Ruth}/d\Omega)(E,\theta_m)}{(d\sigma_{\rm Ruth}/d\Omega)(E,\theta_{\rm tel})}\left(\frac{\Delta\Omega_m}{\Delta\Omega_{\rm tel}}\right), \quad (1)$$

where $Y_{\rm el}$ is the yield of elastic scattering only, obtained from the double Gaussian fit, and Y_m is the average yield of the monitor detectors. The factor $(d\sigma_{\rm Ruth}/d\Omega)(E,\theta_m)$ $[(d\sigma_{\rm Ruth}/d\Omega)(E,\theta_{\rm tel})]$ corresponds to the differential Rutherford scattering cross section for a particular beam energy E, at a monitor angle θ_m (or telescope detector $\theta_{\rm tel}$). The factor $\Delta\Omega_m/\Delta\Omega_{\rm tel}$ is the solid angle ratio of the monitor and telescope detectors. The ratio has been obtained independently for the four $\Delta E-E$ telescope detectors from the lowest forward angles (30°−40°) of the lowest beam energy of 23 MeV, where the scattering is purely Rutherford. The mentioned energy is well below the Coulomb barrier of the system and therefore the elastic scattering in this energy is entirely Rutherford scattering, especially at the lower angles.

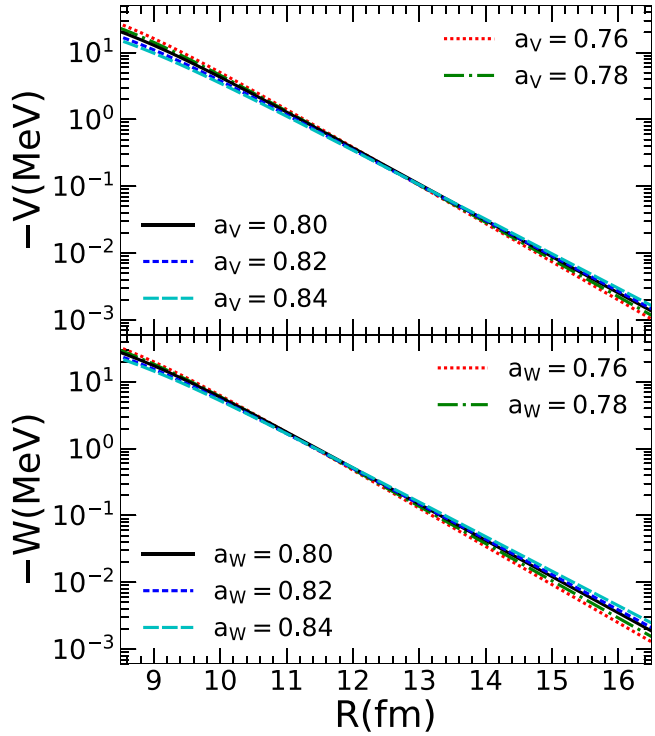

FIG. 4. Sets of different potential parameters that can produce good fit results (shown for $E_{\rm lab} = 35$ MeV). Intersection of the potentials generated by the obtained set of potential parameters are the estimated (a) $R_{\rm Sr}$ and (b) $R_{\rm Si}$. See text for further explanation.

C. Search for the model potential parameters

The calculated ratios of elastic to Rutherford differential scattering cross sections have been used as the input data in the search code SFRESCO [41]. The initial set of potential parameters is derived from the global potential parameters of ^{6}Li, determined by Cook [39]. The resultant potential parameters are $V_0 = 109.5$ MeV, $r_V = 1.326$ fm, $a_V = 0.811$ fm, $W_0 = 24.96$ MeV, $r_W = 1.534$ fm, and $a_W = 0.884$ fm.

The highest energy data at $E_{\rm lab} = 35$ MeV was chosen to optimize the fitting procedure. To avoid the fitting with a large number of parameters at a time, the radius and diffusivity of real (r_V, a_V) and imaginary (r_W, a_W) potentials were kept fixed while the strengths of the volume potentials were varied to obtain the best fit. Afterward, a grid search on the diffusivity parameters were performed within a range from 0.74–0.84 fm to observe a minimum in reduced χ^2 value. Several sets of potential parameters provided good fit, among which, the optimum reduced $\chi^2 = 2.98$ was considered as the best-fit result. The values of sensitivity radii $R_{\rm Sr} = 12.69$ fm and $R_{\rm Si} = 11.45$ fm for real and imaginary parts, respectively, have been calculated from the intersection of different potential parameter sets and shown in Fig. 4. Average value of $R_{\rm Sr}$ and $R_{\rm Si}$, i.e., 12.07 fm has been considered as the mean sensitivity radius.

TABLE I. Optical model potential parameters corresponding to best fit at different energies for the ^{6}Li + ^{159}Tb system. The potential is of Woods-Saxon form with total potential given by $V + iW$. χ^2/n is the reduced χ^2 where n is the number of data points at each energy.

E_{lab} (MeV)	a_V (fm)	a_W (fm)	r_V (fm)	r_W (fm)	V_0 (MeV)	W_0 (MeV)	χ^2/n	σ_R (mb)
25	0.8	0.8	1.09	1.1	78 ± 14	110 ± 11	5.507	632.65
27	0.8	0.8	1.09	1.1	77 ± 6	122 ± 7	1.43	893.13
30	0.8	0.8	1.09	1.1	75 ± 7	95 ± 12	1.023	1164.63
35	0.8	0.8	1.09	1.1	66 ± 3	82 ± 6	2.98	1537.84

The potential parameters at other energies, both below and above the Coulomb barrier, have been obtained by following a similar procedure. Parameters corresponding to the best fit at each energy have been provided in Table I. The values of a_i and r_i (i= real, imaginary) are kept fixed for all energies. The optical model potential has exhibited an energy dependence that is evident from the values in Table I. But, the nature of the energy dependence could not be investigated explicitly due to the unavailability of sufficient angular distribution data at more energies. The angular distributions of elastic-scattering cross section at different energies along with the best fit obtained from SFRESCO have been shown in Fig. 5.

III. THEORETICAL CALCULATIONS

A. Coupled-channel calculation

So far, the statistical estimation of purely elastic contribution generated by the average interaction potential of ^{6}Li + ^{159}Tb has been considered for the phenomenological calculations. However, it is important to probe the reliability of the model potential parameters thus obtained. For this purpose, the total contributions coming from elastic, as well as inelastic, states of ^{159}Tb have been compared with the coupled-channel (CC) calculations using the phenomenologically obtained potential parameters. The quasielastic scattering cross section does not include the contribution from ^{7}Li (see Fig. 1), the n-pickup channel. Moreover, the reproduction of the quasielastic data is necessary to justify the process of extracting the elastic-scattering cross section from the quasielastic scattering data.

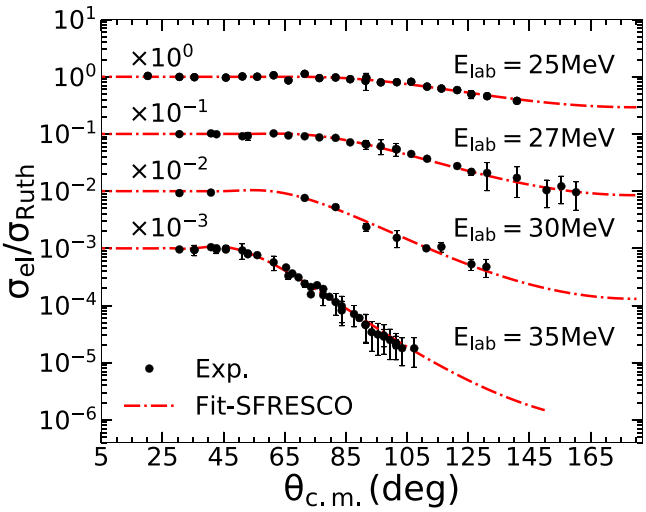

FIG. 5. Extracted angular distribution of differential elastic-scattering cross section ($\sigma_{el}/\sigma_{Ruth}$) at different energies below and above Coulomb barrier. The best fit, corresponding to minimum reduced χ^2, has been obtained from fit with SFRESCO.

TABLE II. Spin-parity (J^π) and energy of states for ^{6}Li + ^{159}Tb system which has been used for calculation.

^{6}Li		^{159}Tb	
J^π	E (keV)	J^π	E (keV)
1^+	g.s.	$\frac{3}{2}^+$	g.s.
		$\frac{5}{2}^+$	57.99
		$\frac{7}{2}^+$	137.5
6		$\frac{9}{2}^+$	241.5

The coupled-channel (CC) calculation has been performed by coupling the ground state (g.s.) and the first two excited states (e.s.) of the target ^{159}Tb with the g.s. of projectile ^{6}Li [42,43] (see Table II), thereby calculating the elastic as well as the inelastic contribution due to the first two e.s. of ^{159}Tb. The excitation of the projectile has not been included within the calculation as ^{6}Li has no other bound state. The results of CC calculation have been compared with experimental quasielastic scattering angular distribution. The CC calculation has been performed using the code FRESCO [41].

For CC calculations, experimental reduced transition probabilities $B(E2)$ for different e.s. of the target ^{159}Tb [43] has been used as input parameters. Collective excitation of the target within the rotational model has been considered. The code FRESCO takes $B(E2)$ value in the unit of e^2 fm^4 which is related to the reduced transition strength in Weisskopf units (W.u.) as

$$B(E2)_{\text{W.u.}} = 0.059\,40 A^{4/3}\, e^2\,\text{fm}^4. \quad (2)$$

For the present calculation, the g.s. and the first two e.s. of ^{159}Tb have been included. The reduced nuclear deformation length for the transitions ($RDEF$) have also been calculated in the rotational model and included as input parameters. Table III consists of the experimental $B(E2)$ values and the calculated $RDEF$ for ^{159}Tb.

TABLE III. Values of inelastic transition elements for ^{159}Tb that has been used for calculation. I_f and I_i are the spins of final and initial states, respectively. E_γ is the γ-ray energy for transition between two states.

$I_f \leftrightarrow I_i$	E_γ (keV)	$B(E2)$ (W.u.)	$RDEF$ (fm)
$3/2 \leftrightarrow 5/2$	57.99	365	3.75
$5/2 \leftrightarrow 7/2$	79.51	240	3.52
$3/2 \leftrightarrow 7/2$	137.5	142	2.71
$7/2 \leftrightarrow 9/2$	103.6	118	2.76
$5/2 \leftrightarrow 9/2$	183.1	220	3.77

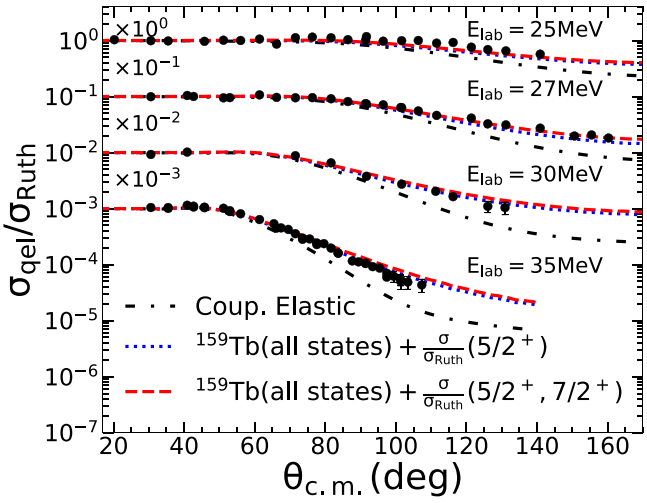

FIG. 6. Quasielastic scattering angular distribution for ^{6}Li + ^{159}Tb system at different energies. The experimental data has been compared with the CC calculations. The addition of first-excited state ($5/2^{+}$) to the elastic scattering cross sections was required to reproduce the experimental quasielastic scattering cross-section. Incorporating the second-excited state ($7/2^{+}$) did not change the theoretical cross sections significantly. Higher excited states of ^{159}Tb has even smaller contributions to the overall cross sections, and thus were not included in the figure.

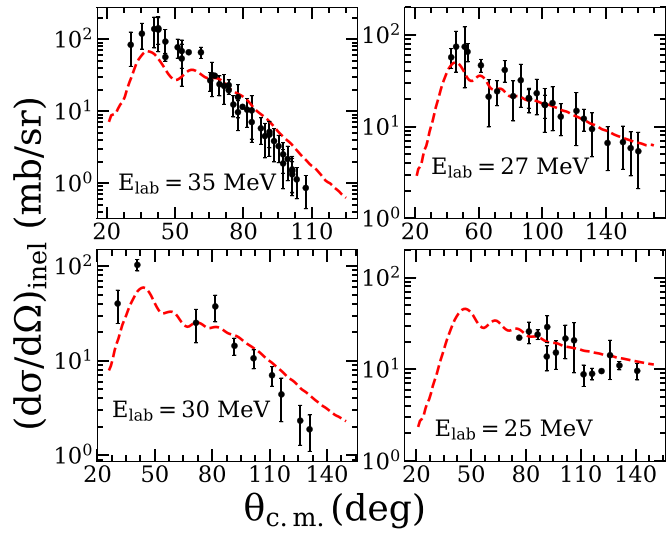

FIG. 7. Inelastic-scattering angular distribution for ^{6}Li + ^{159}Tb ($5/2^{+}$, 58 keV) at different energies. The extracted inelastic cross sections are shown by dots, along with estimated errors. The dashed line represents the inelastic-scattering cross-section angular distribution obtained from CC calculation.

B. Comparison with quasielastic-scattering angular distribution

The effect of coupling on quasielastic-scattering angular distribution has been shown in Fig. 6. The cross sections of the first two e.s. at different angles obtained from the CC calculations have been added with the elastic scattering cross-section angular distribution. The addition of the first e.s. ($5/2^{+}$) is required to reproduce the experimental quasielastic scattering cross section. The addition of the second e.s. does not change the cross sections significantly. The third e.s. is 241 keV apart, and the ΔE-E detectors should be able to resolve any contribution occurring from that state (resolution of the ΔE-E detectors are ≈150 keV). So, the cross section of the third excited state was not added. The addition of the inelastic-scattering cross sections of the first two excited states was required to reproduce the experimental quasielastic scattering cross section.

C. Comparison with inelastic-scattering angular distribution

The inelastic-scattering from the first-excited state (58 keV) that was extracted from the quasielastic band (see Fig. 2) has been compared independently with that calculated by the CC calculation in Fig. 7, at different energies. However, the extraction process becomes more intractable with decreasing energies for reasons described in Sec. II, especially at $E_{\rm lab}$ = 25 MeV. At this energy, a comparison between the CC calculation and extracted inelastic cross section was not attainable for a broad angular range. At the higher energies, the comparison yields an overall satisfactory result. The contribution of the second-excited state could not be compared following a similar procedure as that part could not be extracted from experimental data. The contribution of the second-excited state can be observed in Fig. 6.

D. Finite-range coupled-channel Born approximation

For transfer reactions of type $A + B(B' + X) \rightarrow (A + X) + B'$ (where X is the particle transferred from B to A), the theoretically calculated differential cross section $d\sigma/d\Omega_{\rm th}$ is related to the experimental cross section as

$$\frac{d\sigma}{d\Omega}_{\rm expt} = (C^2S)_{AX}(C^2S)_{B'X}\frac{d\sigma}{d\Omega}_{\rm th}, \tag{3}$$

where C^2 is the isospin Clebsch-Gordan coefficients and S is the spectroscopic factor of the cluster configurations. The product C^2S bears information regarding the probability of a nucleus to be found in a specific configuration. The framework of finite-range coupled-channel Born approximation (CCBA) [44] has been chosen to describe the $1n$ pickup reaction by ^{6}Li from well-deformed ^{159}Tb target nucleus. The rationale behind the choice of the model is the significant probability of two-step processes, like one of the nuclei in the incident channel getting inelastically excited, followed by particle transfer from the state.

In the present work, the CCBA calculation on $1n$ pickup by ^{6}Li from the ^{159}Tb target nucleus has been performed. The experimental cross sections were obtained from the ^{7}Li blob in the two-dimensional (2D) spectrum shown in Fig. 1. The Q value of the reaction and the kinematical calculation suggest that the ^{7}Li band is within the energy window expected from the $1n$ pickup by ^{6}Li. The ^{7}Li band was distinguishable for $E_{\rm lab}$ = 27, 30, and 35 MeV.

A schematic diagram of the coupling scheme for the CCBA calculation is presented in Fig. 8. The first and second inelastic excitations of ^{159}Tb nucleus along with its g.s. are first coupled with ^{6}Li g.s., as described previously. The third excited state at

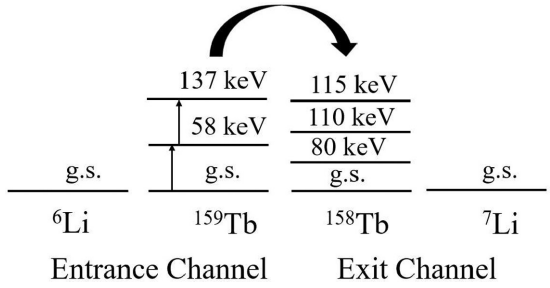

FIG. 8. Schematic diagram of the CCBA calculation performed for $^{6}\mathrm{Li}+{}^{159}\mathrm{Tb}^{*}\rightarrow{}^{7}\mathrm{Li}+{}^{158}\mathrm{Tb}^{*}$ reaction. See text for detailed description.

241.5 keV has a small contribution to transfer cross sections. Therefore, it was not included during the transfer calculations. Following the reaction $^{159}\mathrm{Tb}^{*}(^{6}\mathrm{Li},{}^{7}\mathrm{Li})\,^{158}\mathrm{Tb}^{*}$, the residual ^{158}Tb nucleus can end up either in its g.s. or e.s. [45]. The J^{π} values and energies of those states are listed in Table IV. For a comprehensive analysis, cross sections of the g.s.and the e.s. of ^{158}Tb need to be calculated. In addition, five sets of potential are required for the calculation which are listed below:

(i) Entrance channel $^{6}\mathrm{Li}+{}^{159}\mathrm{Tb}$ potential: obtained from calculations in the previous section.
(ii) Exit channel $^{7}\mathrm{Li}+{}^{158}\mathrm{Tb}$ potential: obtained from Ref. [26]. These potentials are originally for $^{7}\mathrm{Li}+{}^{159}\mathrm{Tb}$ system, but due to the unavailability of $^{7}\mathrm{Li}+{}^{158}\mathrm{Tb}$ potential, the parameters from Ref. [26] have been used.
(iii) Neutron bound state of the target ($^{158}\mathrm{Tb}+n$): potential parameters of Ref. [46] used.
(iv) Neutron bound state of the projectile ($^{6}\mathrm{Li}+n$): potential parameters obtained from Ref. [47].
(v) Core-core potential ($^{6}\mathrm{Li}+{}^{158}\mathrm{Tb}$): the parameters obtained in previous sections were used. The actual "*core-core interaction potential*" might differ from the used value but such potential parameters are unavailable in the literature. The parameters have been altered to extremes (V_0 and W_0 changed from 10–200 MeV) to check their sensitivity on calculated cross sections. The cross sections did not alter to a significant extent, and the nature of the angular distributions occurring from different partitions remained the same.

TABLE IV. J^{π} and energy values of the ground and excited states for ^{158}Tb nucleus which have been used for calculation.

J^{π}	E (keV)
3^{-}	g.s.
4^{-}	79.9
0^{-}	110
1^{-}	115

TABLE V. Spectroscopic factors of the possible bound-state configurations for ^{7}Li and ^{159}Tb [$^{158}\mathrm{Tb}(3^{-},\ \mathrm{g.s.})+n$]. Each partition in the table is individually employed for CCBA calculation. $C^{2}S_{^{158}\mathrm{Tb}+n}$ was initially fixed at 1.0. The best fit provided the estimated value of $C^{2}S_{^{158}\mathrm{Tb}+n}$ (in column 4).

Nucleus	E_x (keV)	State (nlj)	$C^{2}S$ (this work)
^{158}Tb	g.s.	$^{3}p_{3/2}$	0.55 ± 0.05
		$^{2}f_{7/2}$	0.55 ± 0.05
		$^{2}f_{5/2}$	0.55 ± 0.05
	79.9	$^{2}f_{5/2}$	0.55 ± 0.05
	110.0	$^{3}p_{3/2}$	0.55 ± 0.05
		$^{2}f_{5/2}$	0.55 ± 0.05
		$^{2}f_{7/2}$	0.55 ± 0.05
	115.0	$^{3}p_{3/2}$	0.55 ± 0.05

The spectroscopic factor ($C^{2}S$) for $^{6}\mathrm{Li}+n$ configuration of ^{7}Li is found in the literature [48]. But, in view of the unavailability of $C^{2}S$ values for $^{158}\mathrm{Tb}+n$ configuration, the same values have been obtained at first from the experimental cross section at $E_{\mathrm{lab}}=35$ MeV. Theoretical calculations have been performed at that energy for different spectroscopic configurations of $^{158}\mathrm{Tb}+n$ bound states; exclusively, each with initial $C^{2}S=1.0$. The possible configurations for $^{158}\mathrm{Tb}+n$ bound states are presented in Table V with their respective $C^{2}S$ values. Performing CCBA for $^{159}\mathrm{Tb}^{*}(^{6}\mathrm{Li},{}^{7}\mathrm{Li})\,^{158}\mathrm{Tb}$ (g.s.) was not sufficient to reproduce the experimental data. Thus the $^{159}\mathrm{Tb}^{*}(^{6}\mathrm{Li},{}^{7}\mathrm{Li})\,^{158}\mathrm{Tb}^{*}$ (79.9, 110.0, 115.0 keV) coupling schemes were also included in the calculation. Figure 9

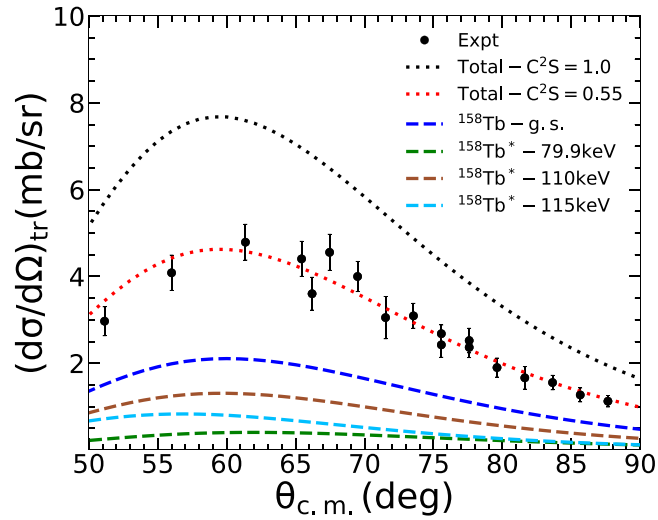

FIG. 9. Experimental angular distribution for $^{159}\mathrm{Tb}^{*}(^{6}\mathrm{Li},{}^{7}\mathrm{Li})\,^{158}\mathrm{Tb}^{*}$ (black dots) at $E_{\mathrm{lab}}=35$ MeV is fit with individual theoretical results occurring from different residual states of ^{158}Tb. All of the individual angular distributions have been calculated with $C^{2}S=1.0$ (dotted and dashed-dot lines). The best fit (black solid line) has been obtained with $C^{2}S=0.55\pm0.5$ for different spectroscopic configurations for $^{159}\mathrm{Tb}\rightarrow{}^{158}\mathrm{Tb}+n$ bound state.

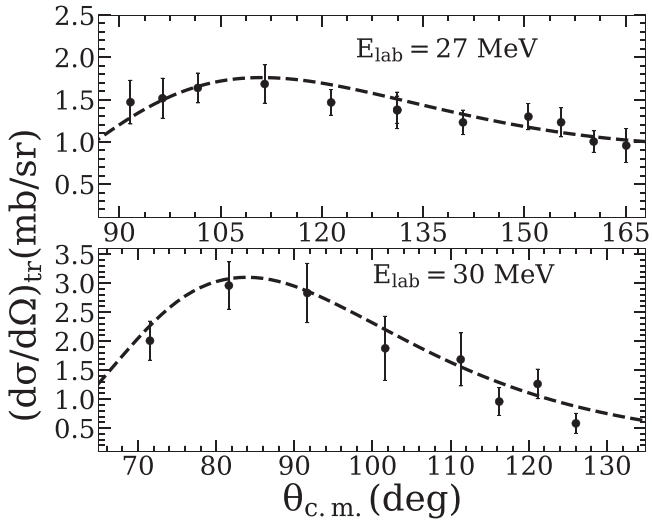

FIG. 10. Experimental cross section for $1n$ pickup reaction ^{159}Tb*(^{6}Li, ^{7}Li)^{158}Tb* (black dots) at $E_{\rm lab} = 27$ and 30 MeV; compared with CCBA calculations (black dashed lines); using the spectroscopic configurations in Table V.

represents the experimental and theoretical differential scattering cross sections for the $1n$ pickup [$(d\sigma/d\Omega)_{\rm tr}$] at $E_{\rm lab} =$ 35 MeV. Experimentally, it was not possible to distinguish the different states of ^{158}Tb*. Hence, a single $C^2S = 0.55 \pm 0.05$ was used for each state to match the experimentally obtained $1n$ pickup cross sections.

The CCBA calculations at $E_{\rm lab} = 27$ and 30 MeV was performed with the obtained $C^2S_{^{158}{\rm Tb}+n}$ values and compared with the experimental data in Fig. 10. Good results have been obtained in both energies, which can be considered as the credibility of the obtained values. Below 27 MeV, the ^{7}Li band could not be separated from ^{6}Li band, experimentally, prohibiting further study of the below barrier $1n$ pickup reaction.

IV. SUMMARY

The quasielastic scattering angular distributions have been measured at energies above and below the Coulomb barrier for ^{6}Li + ^{159}Tb system. The pure elastic scattering cross sections have been extracted from the quasielastic cross sections. The optical model potential parameters have been obtained from the extracted elastic-scattering cross section angular distribution, at each energy. The coupled-channel calculation has been performed, including the coupling with the first three excited states of ^{159}Tb target, and no projectile excitation. The extracted optical model potential parameters are used for the calculation. A reasonable agreement has been achieved between experimental and theoretical quasielastic and inelastic cross sections.

The cross sections for the $1n$ pickup channel for the reaction have been studied. The ^{159}Tb $\rightarrow$ ^{158}Tb $+n$ spectroscopic factors have been estimated from $E_{\rm lab} = 35$ MeV angular distribution data, with the aid of the CCBA calculation. The calculated energy variation of the $1n$ pickup cross sections agree well with that of the experimental cross sections. To match the theoretical and experimental cross sections, a $C^2S = 0.55 \pm 0.5$ was required. Overall, the quality of the fits to the reaction channels within the coupled channel's framework highlights the correctness of the extraction of the elastic-scattering cross section and the resultant optical model parameters for the ^{6}Li + ^{159}Tb system. Experimental measurement spanning a wide energy range can return a comprehensive result regarding the values of different parameters, estimated in this work.

ACKNOWLEDGMENTS

The authors sincerely thank the staff of BARC-TIFR Pelletron facility for an uninterrupted supply of beam. S.B. would like to thank Professor S. Kailas of CBS, Mumbai and Dr. Rajkumar Santra of VECC, Kolkata for discussion on theoretical frameworks that have been employed in this work.

[1] A. Pakou, N. Alamanos, A. Lagoyannis, A. Gillibert, E. C. Pollacco, P. A. Assimakopoulos, G. Doukelis, K. G. Ioannides, D. Karadimos, D. Karamanis *et al.*, Phys. Lett. B **556**, 21 (2003).

[2] A. Pakou, N. Alamanos, G. Doukelis, A. Gillibert, G. Kalyva, M. Kokkoris, S. Kossionides, A. Lagoyannis, A. Musumarra, C. Papachristodoulou *et al.*, Phys. Rev. C **69**, 054602 (2004).

[3] A. Pakou, Phys. Rev. C **78**, 067601 (2008).

[4] N. Keeley, S. J. Bennett, N. M. Clarke, B. R. Fulton, G. Tungate, P. V. Drumm, M. A. Nagarajan, J. S. Lilley *et al.*, Nucl. Phys. A **571**, 326 (1994).

[5] A. M. M. Maciel, P. R. S. Gomes, J. Lubian, R. M. Anjos, R. Cabezas, G. M. Santos, C. Muri, S. B. Moraes, R. Liguori Neto, N. Added *et al.*, Phys. Rev. C **59**, 2103 (1999).

[6] J. Lubian, T. Correa, B. Paes, J. M. Figueira, D. Abriola, J. O. Fernández Niello, A. Arazi, O. A. Capurro, E. de Barbará, G. V. Martí *et al.*, Nucl. Phys. A **791**, 24 (2007).

[7] M. S. Hussein, P. R. S. Gomes, J. Lubian, and L. C. Chamon, Phys. Rev. C **73**, 044610 (2006).

[8] P. R. S. Gomes, I. Padron, J. O. Fernández Niello, G. V. Martí, M. D. Rodríguez, O. A. Capurro, A. J. Pacheco, J. E. Testoni, A. Arazi, J. Lubian *et al.*, J. Phys. G **31**, S1669 (2005).

[9] S. B. Moraes, P. R. S. Gomes, J. Lubian, J. J. S. Alves, R. M. Anjos, M. M. Sant'Anna, I. Padrón, C. Muri, R. Liguori Neto, and N. Added, Phys. Rev. C **61**, 064608 (2000).

[10] R. J. Woolliscroft, B. R. Fulton, R. L. Cowin, M. Dasgupta, D. J. Hinde, C. R. Morton, and A. C. Berriman, Phys. Rev. C **69**, 044612 (2004).

[11] P. R. S. Gomes, R. M. Anjos, C. Muri, J. Lubian, I. Padron, L. C. Chamon, R. Liguori Neto, N. Added, J. O. Fernández Niello, G. V. Martí, et al., Phys. Rev. C **70**, 054605 (2004).

[12] P. R. S. Gomes, M. D. Rodríguez, G. V. Martí, I. Padron, L. C. Chamon, J. O. Fernández Niello, O. A. Capurro, A. J. Pacheco, J. E. Testoni, A. Arazi *et al.*, Phys. Rev. C **71**, 034608 (2005).

[13] P. R. S. Gomes, I. Padron, E. Crema, O. A. Capurro, J. O. Fernández Niello, A. Arazi, G. V. Martí, J. Lubian, M. Trotta, A. J. Pacheco *et al.*, Phys. Rev. C **73**, 064606 (2006).

[14] J. M. Figueira, D. Abriola, J. O. Fernández Niello, A. Arazi, O. A. Capurro, E. de Barbará, G. V. Martí, D. Martínez Heimann, A. J. Pacheco *et al.*, Phys. Rev. C **73**, 054603 (2006).
[15] J. M. Figueira, J. O. Fernández Niello, D. Abriola, A. Arazi, O. A. Capurro, E. de Barbará, G. V. Martí, D. Martínez Heimann, A. E. Negri, A. J. Pacheco *et al.*, Phys. Rev. C **75**, 017602 (2007).
[16] J. M. Figueira, J. O. Fernández Niello, A. Arazi, O. A. Capurro, P. Carnelli, L. Fimiani, G. V. Martí, D. Martinez Heimann, A. E. Negri, A. J. Pacheco *et al.*, Phys. Rev. C **81**, 024613 (2010).
[17] A. Gómez Camacho, P. R. S. Gomes, J. Lubian, and I. Padrón, Phys. Rev. C **77**, 054606 (2008).
[18] H. Kumawat, V. Jha, B. J. Roy, V. V. Parkar, S. Santra, V. Kumar, D. Dutta, P. Shukla, L. M. Pant, A. K. Mohanty *et al.*, Phys. Rev. C **78**, 044617 (2008).
[19] C. Signorini, A. Andrighetto, M. Ruan, J. Y. Guo, L. Stroe, F. Soramel, K. E. G. Löbner, L. Müller, D. Pierroutsakou, M. Romoli *et al.*, Phys. Rev. C **61**, 061603(R) (2000).
[20] M. Zadro, P. Figuera, A. Di Pietro, F. Amorini, M. Fisichella, O. Goryunov, M. Lattuada, C. Maiolino, A. Musumarra, V. Ostashko *et al.*, Phys. Rev. C **80**, 064610 (2009).
[21] M. Biswas, Subinit Roy, M. Sinha, M. K. Pradhan, A. Mukherjee, P. Basu, H. Majumdar, K. Ramachandran, and A. Shrivastava, Nucl. Phys. A **802**, 67 (2008).
[22] E. F. Aguilera, E. Martinez-Quiroz, D. Lizcano, A. Gómez-Camacho, J. J. Kolata, L. O. Lamm, V. Guimarães, R. Lichtenthäler, O. Camargo, F. D. Becchetti *et al.*, Phys. Rev. C **79**, 021601(R) (2009).
[23] A. R. Garcia, J. Lubian, I. Padron, P. R. S. Gomes, T. Lacerda, V. N. Garcia, A. Gómez Camacho, E. F. Aguilera *et al.*, Phys. Rev. C **76**, 067603 (2007).
[24] N. Yu, H. Q. Zhang, H. M. Jia, S. T. Zhang, M. Ruan, F. Yang, Z. D. Wu, X. X. Xu, C. L. Bai *et al.*, J. Phys. G **37**, 075108 (2010).
[25] N. N. Deshmukh, S. Mukherjee, D. Patel, N. L. Singh, P. K. Rath, B. K. Nayak, D. C. Biswas, S. Santra, E. T. Mirgule, L. S. Danu *et al.*, Phys. Rev. C **83**, 024607 (2011).
[26] D. Patel, S. Mukherjee, D. C. Biswas, B. K. Nayak, Y. K. Gupta, L. S. Danu, S. Santra, and E. T. Mirgule, Phys. Rev. C **91**, 054614 (2015).
[27] Y. Y. Yang, X. Liu, and D. Y. Pang, Phys. Rev. C **94**, 034614 (2016).
[28] M. Mazzocco, N. Keeley, A. Boiano, C. Boiano, M. La Commara, C. Manea, C. Parascandolo, D. Pierroutsakou, C. Signorini, E. Strano *et al.*, Phys. Rev. C **100**, 024602 (2019).
[29] H. Kumawat, C. Joshi, V. V. Parkar, V. Jha, B. J. Roy, Y. S. Sawant, P. C. Rout, E. T. Mirgule, R. K. Singh, N. L. Singh *et al.*, Nucl. Phys. A **1002**, 121973 (2020).
[30] L. F. Canto, P. R. S. Gomes, R. Donangelo, and M. S. Hussein, Phys. Rep. **424**, 1 (2006).
[31] P. R. S. Gomes, J. Lubian, L. F. Canto, D. R. Otomar, D. R. Mendes Junior, P. N. de Faria, R. Linares, L. Sigaud, J. Rangel, J. L. Ferreira *et al.*, Few-Body Syst. **57**, 165 (2016).
[32] G. R. Satchler, Phys. Rep. **199**, 147(1991).
[33] A. A. Aponick Jr., C. M. Chesterfield, D. A. Bromley, and N. K. Glendenning, Nucl. Phys. A **159**, 367 (1970).
[34] J. R. Birkelund, J. R. Huizenga, H. Freiesleben, K. L. Wolf, J. P. Unik, and V. E. Viola, Jr., Phys. Rev. C **13**, 133 (1976).
[35] M. K. Pradhan, A. Mukherjee, P. Basu, A. Goswami, R. Kshetri, Subinit Roy, P. Roy Chowdhury, M. Saha Sarkar, R. Palit, V. V. Parkar, S. Santra, and M. Ray, Phys. Rev. C **83**, 064606 (2011).
[36] M. K. Pradhan, A. Mukherjee, Subinit Roy, P. Basu, A. Goswami, R. Kshetri, R. Palit, V. V. Parkar, M. Ray, M. Saha Sarkar, and S. Santra, Phys. Rev. C **88**, 064603 (2013).
[37] P. Biswas, A. Mukherjee, S. Bhattacharjee, D. Chattopadhyay, Subinit Roy, S. Santra, S. K. Pandit, K. Ramachandran, K. Mahata, and A. Shrivastava, Phys. Rev. C **104**, 034620 (2021).
[38] A. Chatterjee, LAMPS: Linux Advanced Multiparameter System (2008), http://www.tifr.res.in/pell/lamps.html.
[39] J. Cook, Nucl. Phys. A **388**, 153 (1982).
[40] Y. Xu, Y. Han, J. Hu, H. Liang, Z. Wu, H. Guo, and C. Cai, Phys. Rev. C **98**, 024619 (2018).
[41] I. J. Thompson, Comput. Phys. Rep. **7**, 167 (1988).
[42] D. R. Tilley, C. M. Cheves, J. L. Godwin, G. M. Hale, H. M. Hofmann, J. H. Kelley, C. G. Sheu, and H. R. Weller, Nucl. Phys. A **708**, 3 (2002).
[43] C. W. Reich, Nucl. Data Sheets **113**, 157 (2012).
[44] T. Tamura, Phys. Rep. **14**, 59 (1974).
[45] N. Nica, Nucl. Data Sheets **141**, 1 (2017).
[46] F. D. Becchetti and G. W. Greenlees, Phys. Rev. **182**, 1190 (1969).
[47] T. Y. Li and S. K. Mark, Nucl. Phys. A **123**, 147 (1969).
[48] A. T. Rudchik, K. A. Chercas, K. W. Kemper, A. A. Rudchik, S. Kliczewski, E. I. Koshchy, K. Rusek, S. Yu. Mezhevych, O. A. Ponkratenko, Val. M. Pirnak *et al.*, Nucl. Phys. A **927**, 209 (2014).